



A new GVF-based image enhancement formulation for use in the presence of mixed noise

Ovidiu Ghita*, Paul F. Whelan

Centre for Image Processing and Analysis, Dublin City University, Dublin 9, Ireland

ARTICLE INFO

Article history:

Received 11 September 2009

Received in revised form

22 January 2010

Accepted 27 February 2010

Keywords:

Anisotropic diffusion

Shock filters

GVF

Texture enhancement

ABSTRACT

This paper is concerned with the introduction of a new gradient vector flow (GVF) field formulation that shows increased robustness in the presence of mixed noise and with its evaluation when included in the development of image enhancement algorithms. In this regard, the main contribution associated with this work resides in the development of an adaptive image enhancement framework that couples the anisotropic diffusion models with the adaptive median filtering that is designed for the restoration of digital images corrupted with mixed noise. To further illustrate the advantages associated with the proposed GVF field formulation, additional experiments are conducted when the proposed strategy is applied in the construction of anisotropic models for texture enhancement.

© 2010 Elsevier Ltd. All rights reserved.

1. Introduction

Image enhancement is one of the fundamental topics of research in computer vision. As a result of this interest from the computer vision community, a large number of approaches have been proposed where the main goal was the implementation of feature preserving noise removal and image enhancement strategies. The majority of the existing noise removal algorithms assumes that the image noise has two main characteristics, it has either a Gaussian distribution or it is of impulse type, and as a result substantial research efforts have been devoted to address the optimal restoration of digital images that are corrupted by one particular noise component. In this regard, the anisotropic diffusion approach proposed by Perona and Malik [18] is one representative feature-preserving smoothing strategy that addresses the restoration of images corrupted by Gaussian noise. Since its introduction a large number of studies have been devoted to propose various computational schemes that improve either the numerical stability [2,5,6,10] or the edge preservation performance [4,11,15,16,24] of the original Perona–Malik (P–M) anisotropic diffusion model. In this sense, the introduction of the shock filters by Osher and Rudin [17] opened the possibility to reformulate the image enhancement as a combination of two coupled terms that implement inverse (shock) and forward diffusion processes [1,9]. Another step forward was represented by the incorporation of the gradient vector flow (GVF) field in the implementation of the anisotropic diffusion models. The GVF field has been originally introduced by Xu and Prince [19] in the development of a novel active contour formulation where a new external force model (GVF) has been shown to

circumvent the difficulties faced by the conventional external forces in capturing the shape concavities. This desirable property of the GVF has been investigated in detail in the paper by Yu and Chua [23] where they demonstrated that the GVF field is invariant to the application of the image diffusion process and in addition they proved that the GVF is able to capture more accurately the object boundaries in images corrupted by high levels of Gaussian noise than the anisotropic models based on standard partial differential equations (PDE). However, since the GVF is constructed using a pair of differential equations that diffuse the gradient vectors in orthogonal directions, this PDE model is vulnerable when the image data is corrupted by impulse or mixed noise. In this paper we propose a new version of GVF that shows more stability in the presence of impulse noise. The evaluation of the proposed GVF formulation when applied to image data corrupted by different types of image noise and its inclusion in the development of a new filtering scheme that is able to restore and enhance images corrupted by mixed noise represent the main contributions associated with this work. This paper is organised as follows. Section 2 introduces a new GVF formulation that is able to adapt to impulse noise. Section 3 details the implementation of a coupled image restoration scheme based on the Alvarez–Mazora [1] anisotropic diffusion. Section 4 presents the experimental results, while Section 5 concludes this paper.

2. Gradient vector flow

In the original implementation [19], the GVF has been defined as the vector field that minimises the following functional:

$$\xi(V) = \int_{\Omega} \mu |\nabla V|^2 + |\nabla f|^2 (V - \nabla f)^2 d\Omega \quad (1)$$

* Corresponding author.

E-mail address: ghitao@eeng.dcu.ie (O. Ghita).

where f is the input image, $V=[u,v]$ is the GVF field, ∇ is the gradient operator and Ω is the image domain. The minimisation of the functional $\xi(V)$ can be achieved using the calculus of variations (see Appendix A for additional details) and the GVF field V can be determined for each pixel in the image as the stationary value of the following iterative equation:

$$V_t = \mu\Delta V - (V - \nabla f) |\nabla f|^2 \tag{2}$$

where V_t is the partial derivative of the GVF with respect to the time variable t and Δ is the Laplacian operator. This formulation can be implemented in a recursive fashion in the discrete domain as follows:

$$\begin{cases} u_t = \mu\Delta u - [u - f_x][f_x^2 + f_y^2] \\ v_t = \mu\Delta v - [v - f_y][f_x^2 + f_y^2] \\ u_{t=0} = f_x, \quad v_{t=0} = f_y \end{cases} \tag{3}$$

where f_x and f_y are the partial derivatives of f with respect to x and y axes. As illustrated in (1)–(3), the GVF field is formed by two terms. The first term performs the diffusion of the edge information in agreement with a regularization parameter μ , while the second term ensures that the GVF field maintains the maximum values at positions in the image where the gradient information is maximised. This property is desirable since the sign of the GVF on both sides of the edge are opposite. Consequently, the intensity of the GVF field shows a progressive descent with the increase in the distance between the pixels situated in the edge neighbourhood with respect to the position where the gradient is maximised. Thus, the incorporation of the edge diffusion process in the development of anisotropic models is advantageous since the GVF field does not attenuate the edge information and allows the application of the data filtering process in an increased region around both sides of the edge

map. Unfortunately, this positive aspect associated with the GVF field is compromised in the presence of impulse noise and this can be clearly visualised in Fig. 1 (image size 128×128).

This behaviour of the GVF field is expected since the aim of the formulation shown in (1) is to preserve the strength of the gradient information. In a recent paper, Xu and Prince [20] tried to address the sensitivity to noise of the original GVF field by replacing the constant term μ with a diffusive term, $\mu \leftarrow g(|\nabla f|)$, and multiply the second term of the GVF with $(1 - g(|\nabla f|))$. It is useful to note that in their paper the authors omitted the term μ in the formulation of the generalized (G)-GVF field. While the diffusion function $g(|\nabla f|) = \exp(-|\nabla f|/K)$ is bounded in the interval $(0,1]$, the regularization term is still necessary to maintain the convergence of the GVF field, unless the time step Δt is reduced in the discrete implementation of the GVF. For more details the reader can refer to Xu and Prince [20]. Nonetheless, this simple modification introduces a spatially varying weighting term that regularizes the edge diffusion process and improves the performance of the GVF field when applied to noisy images corrupted by Gaussian noise, but has virtually no positive influence when the input data is corrupted by impulse noise. If we analyse (1) in detail, we can notice that the second term of the GVF field dominates close to the edge boundaries, as $|\nabla f|^2$ has large values near strong edges, and this term cancels the effect of the first term that implements the edge diffusion process. This behaviour is highly detrimental when the image data is corrupted by impulse noise, as the original and the generalized GVF formulations [12,20] preserve the noisy gradients in the GVF field. Thus, in this paper we focus our attention on the second term of (1) with a view of implementing a new GVF formulation that is able to preserve the field continuity in the presence of impulse noise. In the proposed formulation shown in (4), the second term of the GVF is weighted by the response of an impulse

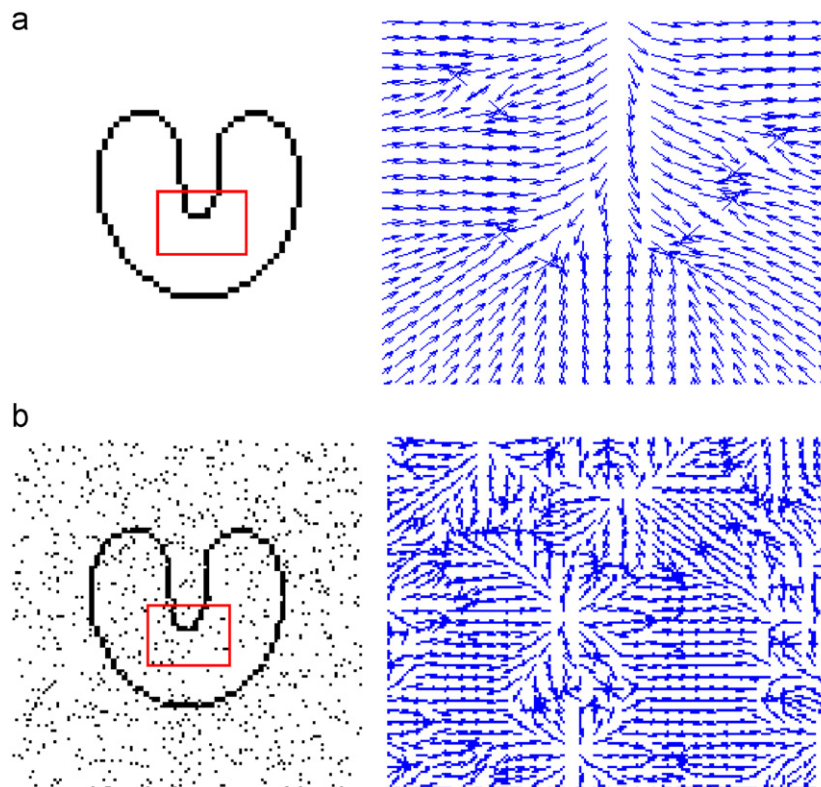


Fig. 1. The GVF field: (a) original image and the corresponding GVF field [19] and (b) image corrupted with impulse noise and the corresponding GVF field. For visualisation purposes the GVF field is displayed only for the region of interest marked with a rectangle in the left image.

noise estimator (IN_{Est}) as follows:

$$\xi(V) = \int_{\Omega} \mu |\nabla V|^2 + IN_{Est}(f) |\nabla f|^2 (V - \nabla f)^2 d\Omega \quad (4)$$

where Ω is the \mathbf{R}^2 image domain. Let ψ be the neighbourhood around the pixel of interest x_{ij} and $X = \{x_{mn} | (m,n) \in \psi\}$ be the set that is constructed by reading the pixels that define ψ in lexicographical order. The impulse noise estimator is implemented based on the assumption that the pixels situated in the local neighbourhood ψ approximate a Gaussian distribution unless the data is corrupted by impulse noise. Using this assumption the impulse noise estimator α can be implemented as follows:

$$\alpha = (x_{ij} - \bar{x})^2 / (2\sigma^2 + \varepsilon) \quad (5)$$

where

$$\bar{x} = \frac{1}{card(\psi)} \sum_{(m,n) \in \psi} x_{mn}$$

and

$$\sigma = \sqrt{\frac{1}{card(\psi)} \sum_{(m,n) \in \psi} (x_{mn} - \bar{x})^2}$$

are the mean and the standard deviation of the pixels contained in the set X , ε is a small value that prevents the division by zero in constant image areas and $card(\psi)$ denotes the cardinality of the set ψ . It can be observed that α takes large values if the central pixel is corrupted by impulse noise and low values for regions with a flat pixel distribution. Nonetheless, the relationship depicted in (4) will also respond to a lesser extent to image details such as edges and to further improve the selectivity of the impulse noise estimator we propose to map the responses generated by (5) using an exponential function as follows:

$$IN_{Est}(x_{ij}) = \exp(-\alpha) \quad (6)$$

It can be observed in (6) that IN_{Est} is a bounded function that takes values in the interval (0,1) and converges to zero when the central pixel of the distribution X is corrupted by impulse noise. To improve the continuity of the GVF field in the local image domain, the impulse

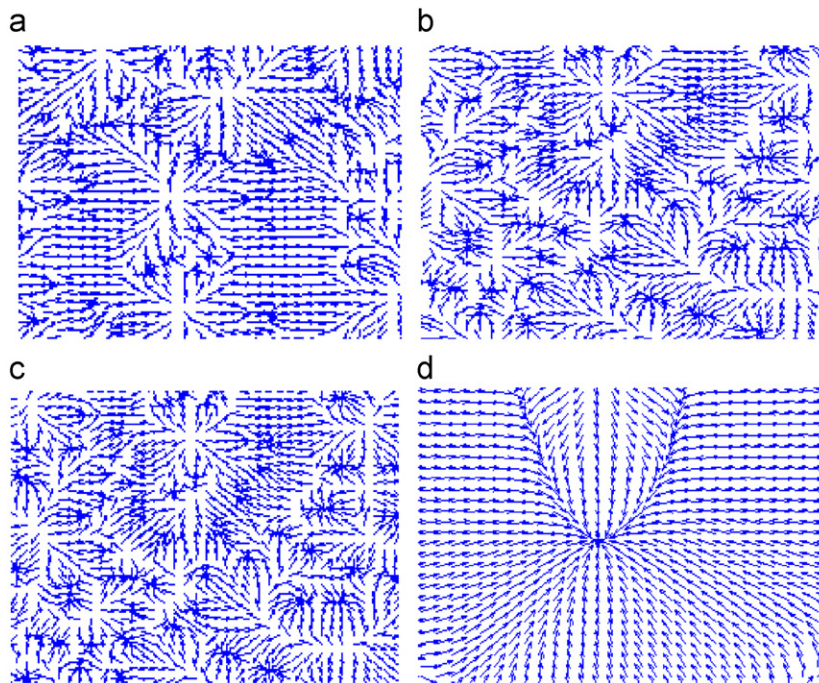


Fig. 2. GVF field calculated for the noisy image shown in Fig. 1: (a) original GVF implementation [19]; (b) generalized G-GVF [20], $K=0.05$; (c) generalized G-GVF [20], $K=0.2$ and (d) Proposed IN_{Est} -GVF ($\mu=0.2$). In all experiments $\Delta t = 1$.



Fig. 3. Results of the image restoration algorithm detailed in Eq. (17): (a) 'Lena' image corrupted with mixed noise (Gaussian noise— $\mathcal{N}(0,20)$, impulse noise—probability 0.1); (b) GVF—Eq. (1)—PSNR 20.39; (c) generalized (G)-GVF—PSNR 20.35 and (d) proposed IN_{Est} -GVF—PSNR 20.65.

noise estimator is calculated as follows:

$$IN_{Est}(x_{ij}) \leftarrow \inf_{\Gamma} (IN_{Est}(f)) \tag{7}$$

where Γ is a local neighbourhood around the central pixel x_{ij} and \inf is the infimum operator. It can be noted that the infimum operator implements a local diffusion for IN_{Est} values calculated with (6) and this allows the edge diffusion term ($\mu|\nabla V|^2$) shown in (4) to dominate in the calculation of the GVF field within the Γ

neighbourhood around the pixels corrupted by impulse noise. Similar to the original [19] and generalised GVF formulations [12,20], the proposed scheme is also convergent if the following relationship that illustrates the mutual dependence between the time step (Δt) and parameter μ is upheld.

$$\Delta t \leq \frac{\Delta x \Delta y}{4\mu} \tag{8}$$

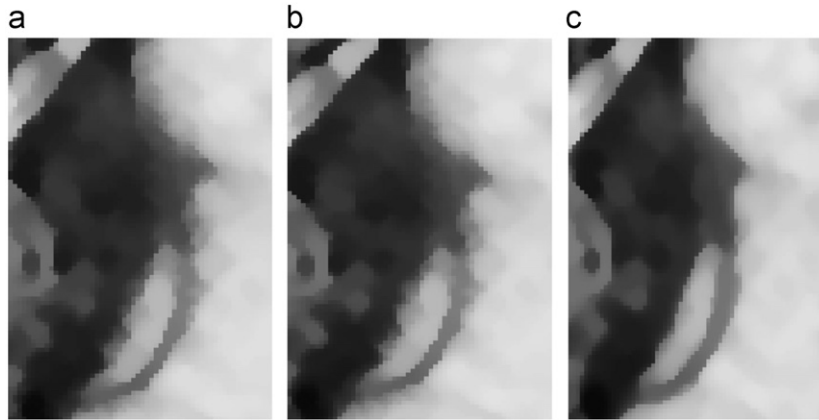


Fig. 4. Close-up details from images depicted in Fig. 3: (a) GVF; (b) G-GVF; (c) IN_{Est} -GVF. Note the improved preservation of the objects' boundaries attained by the IN_{Est} -GVF image restoration scheme.

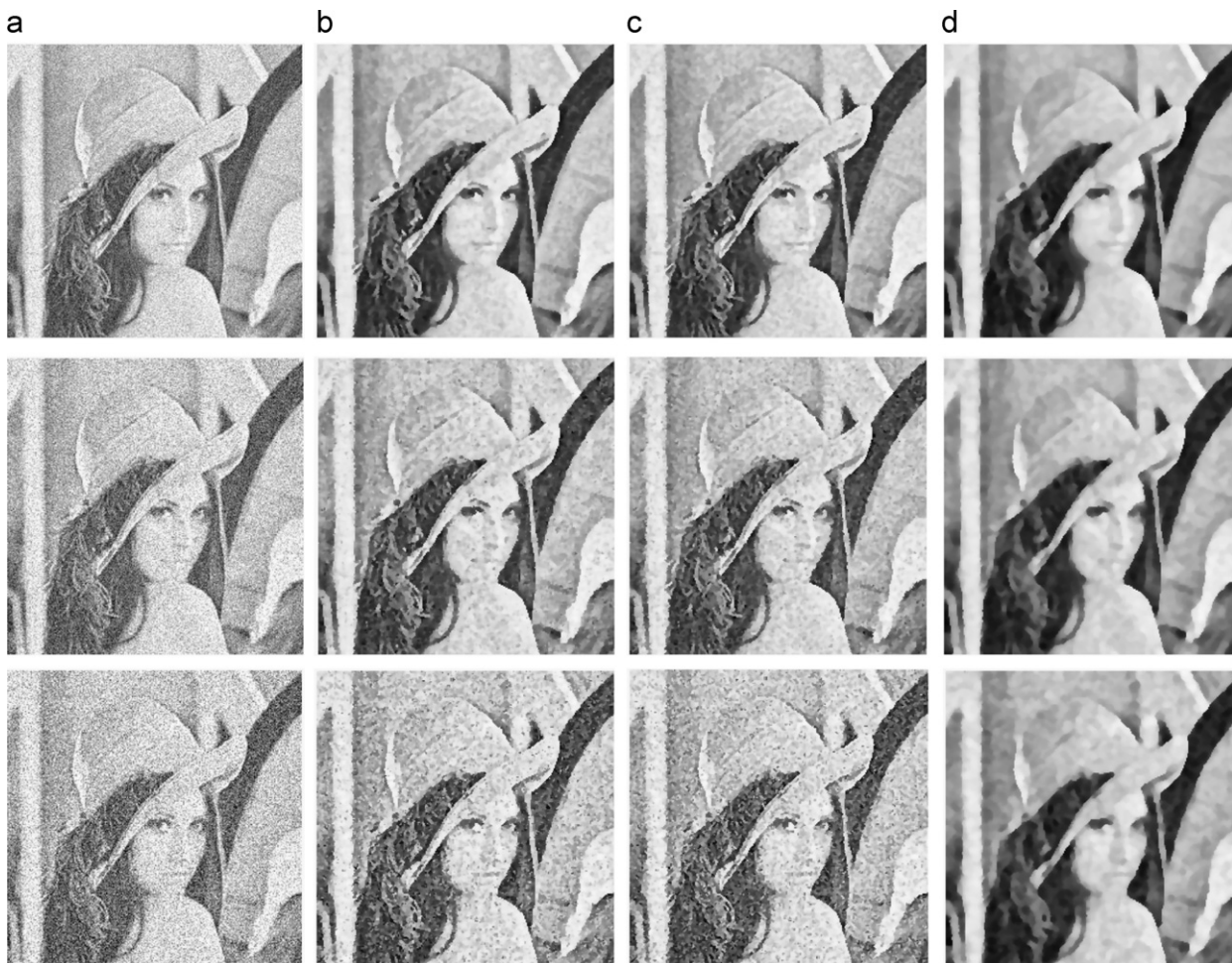


Fig. 5. Experimental results when the image restoration algorithms are applied to 'Lena' image corrupted by Gaussian noise: (a) noisy images: top row $\mathcal{N}(0,20)$, middle row $\mathcal{N}(0,30)$, bottom row $\mathcal{N}(0,40)$; (b) GVF-AM (Eq. 16); (c) G-GVF-AM (Eq. 16) and (d) IN_{Est} -GVF-AM (Eq. 17). PSNR values calculated when the GVF-AM, G-GVF-AM and IN_{Est} -GVF-AM image restoration schemes are applied to 'Lena' image corrupted by different levels of Gaussian noise are depicted in Fig. 7.

Proposition. The IN_{Est} -GVF formulation is convergent if the relationship shown in (8) is upheld.

Proof. (Proof is provided only for the component u of the GVF field since the demonstration is identical for the v component.) The implementation of the IN_{Est} -GVF field (component u) in the discrete domain is shown in (9).

$$u_t = \mu \Delta u - IN_{Est}(f)(u - f_x) |\nabla f|^2 \tag{9}$$

where

$$u_t = \frac{u_{ij}^{n+1} - u_{ij}^n}{\Delta t}, \quad \Delta u = \frac{\sum_{s \in N_4(i,j)} u_s - 4u_{ij}}{\Delta x \Delta y}$$

and $N_4(i,j)$ defines the four connected neighbourhood around the pixel with coordinates (i,j) and the superscript n denotes the iteration index. If we assume that u_{ij}^n is a maxima, then the term $IN_{Est}(f(i,j)) \approx 0$ and (9) can be re-written as follows:

$$u_{ij}^{n+1} = u_{ij}^n - \frac{\mu \Delta t}{\Delta x \Delta y} 4u_{ij}^n + \frac{\Delta t}{\Delta x \Delta y} \sum_{s \in N_4(i,j)} u_s \tag{10}$$

Since u_{ij}^n is a maxima ($0 \leq u_{ij}^{n+1} \leq u_{ij}^n$) and the term

$$\frac{\Delta t}{\Delta x \Delta y} \sum_{s \in N_4(i,j)} u_s \ll u_{ij}^n$$

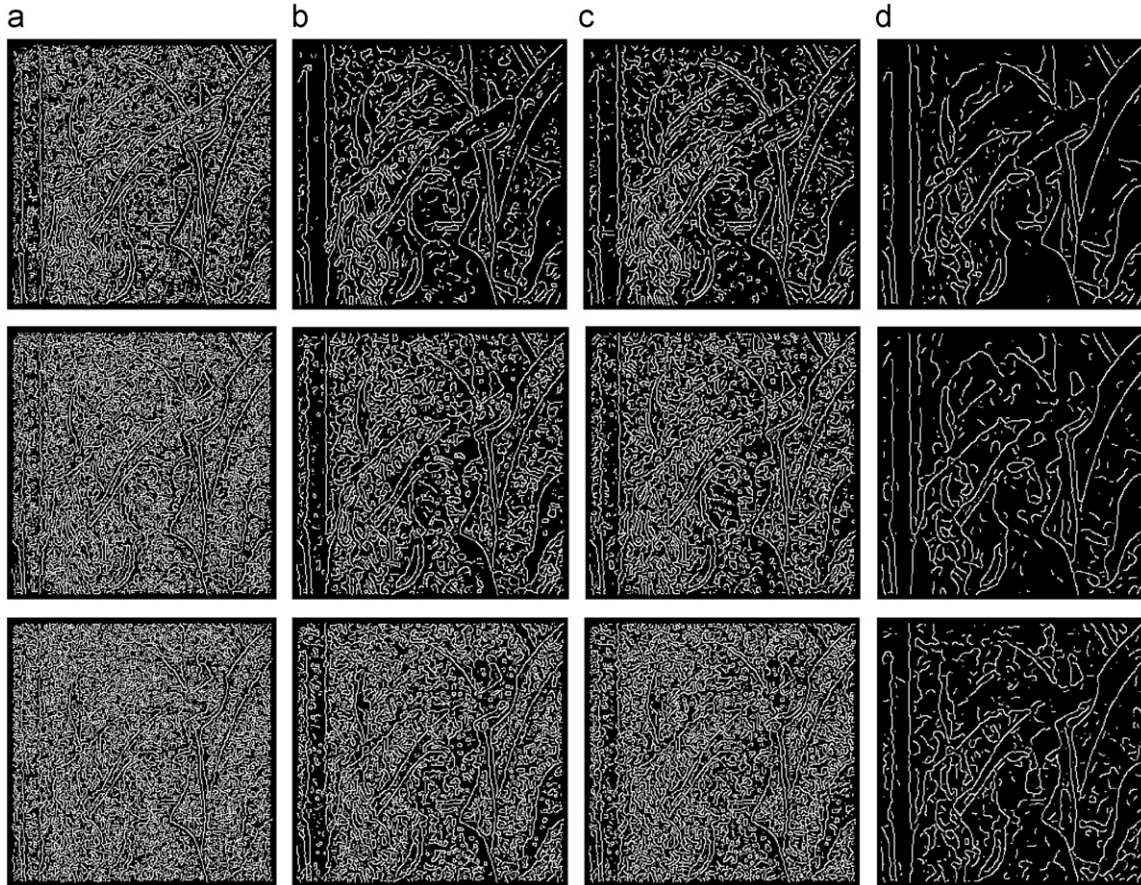


Fig. 6. Edge information extracted using the Canny edge detector (scale parameter=1.0) corresponding to the images shown in Fig. 5: (a) noisy images: top row $\mathcal{N}(0,20)$, middle row $\mathcal{N}(0,30)$, bottom row $\mathcal{N}(0,40)$; (b) GVF-AM (Eq. (16)); (c) G-GVF-AM (Eq. (16)) and (d) IN_{Est} -GVF-AM (Eq. (17)).

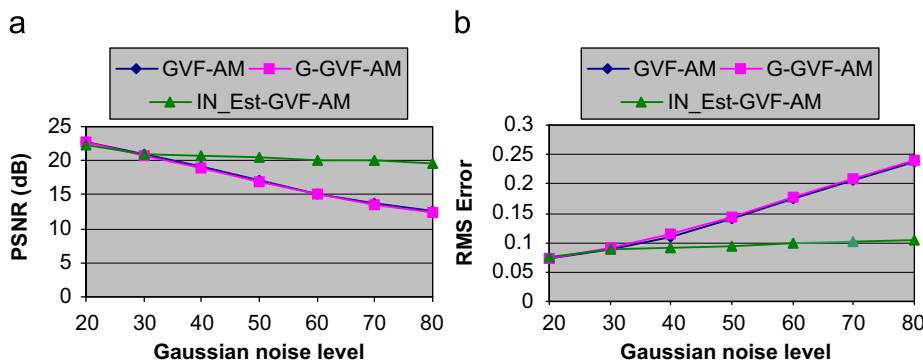


Fig. 7. (a) PSNR values and (b) root mean square (RMS) errors (image data normalised in the interval [0,1]) when the GVF-based Alvarez–Mazora (A–M) anisotropic diffusion schemes analysed in this study are applied to data ('Lena' image) corrupted by different levels of Gaussian noise.

then (10) becomes,

$$0 \leq u_{ij}^n - \frac{\mu \Delta t}{\Delta x \Delta y} 4u_{ij}^n \leq u_{ij}^n \quad (11)$$

While the right hand side of the expression illustrated in (11) is obvious since $-(\mu \Delta t / \Delta x \Delta y) 4u_{ij}^n \leq 0$, we further analyse the left hand side of (11),

$$-u_{ij}^n \leq -(\mu \Delta t / \Delta x \Delta y) 4u_{ij}^n, \text{ if we multiply both sides by } -\frac{1}{u_{ij}^n}, \Rightarrow \Delta t \leq \frac{\Delta x \Delta y}{4\mu} \quad (12)$$

If the spacing between pixels $\Delta x = \Delta y = 1$, then $\Delta t \leq 1/4\mu$. A similar judgement can be applied if the point u_{ij}^n is a minima. If the time step $\Delta t = 1$, then the IN_{Est} -GVF field is convergent if the regularization parameter μ is set to values in the range $[0, 0.25]$.

Fig. 2 illustrates the results of the GVF field when the original, generalized and proposed (IN_{Est} -GVF) formulations are applied to the noisy image shown in Fig. 1. □

The experimental results shown in Fig. 2 indicate, as expected, that the standard GVF (see Eq. (1)) is not able to reject the



Fig. 8. Experimental results when the image restoration algorithms are applied to 'Lena' image corrupted by impulse noise: (a) noisy images: top row—probability 0.1, bottom row—probability 0.2; (b) GVF-AM; (c) G-GVF-AM and (d) IN_{Est} -GVF-AM.

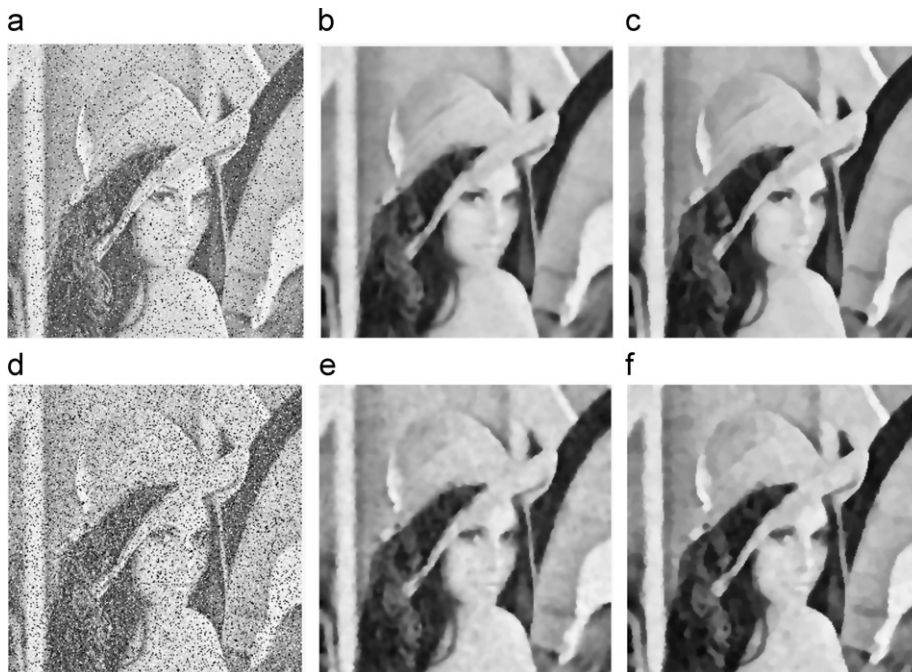


Fig. 9. Experimental results when the proposed image restoration scheme is applied to image data corrupted by mixed noise: (a) noisy image (Gaussian noise— $\mathcal{N}(0,10)$, impulse noise—probability 0.1); (b) filtered image—Yang and Fox [22]—PSNR 20.58; (c) filtered image (IN_{Est} -GVF-AM)—PSNR 20.82; (d) noisy image (Gaussian noise— $\mathcal{N}(0,20)$, impulse noise—probability 0.2); (e) filtered image—Yang and Fox [22]—PSNR 20.48 and (f) filtered image (IN_{Est} -GVF-AM)—PSNR 20.61.

gradients generated by impulse noise. The generalized implementation (G-GVF) [20] shows instability around pixels corrupted by impulse noise and this is more noticeable when the diffusion parameter K is set to larger values. These results are expected since the diffusion function $g(|\nabla f|) = \exp(-|\nabla f|/K)$ that replaces the regularization parameter μ in (1) shows poor stability in the presence of impulse noise (as it evaluates the gradient information). Conversely, the proposed IN_{Est} -GVF formulation shows a much better performance in the presence of impulse noise and its properties prompt us to investigate its usefulness in the implementation of image and texture

enhancement algorithms. This is demonstrated in Fig. 3 where the image restoration scheme detailed in (17) is applied to an image corrupted with mixed noise (combination of Gaussian and impulse noise). For visualisation purposes close-up details are shown in Fig. 4.

3. GVF and anisotropic diffusion-based image enhancement

The application of the diffusion models for image enhancement has been first evaluated by Perona and Malik [18] where

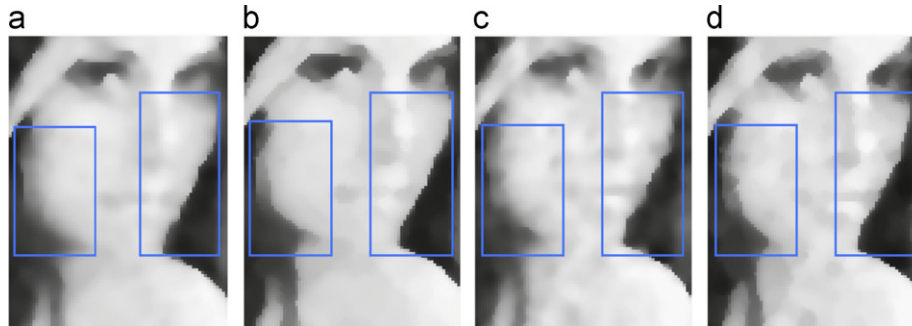


Fig. 10. Close-up details from images depicted in Fig. 9: (a) Yang-Fox [22]—Fig. 9(b); (b) IN_{Est} -GVF-AM—Fig. 9(c); (c) Yang-Fox [22]—Fig. 9(e) and (d) IN_{Est} -GVF-AM—Fig. 9(f). Note the undesired blurring effects generated by Yang and Fox [22] method and the improved preservation of the objects' boundaries attained by the IN_{Est} -GVF-AM image restoration scheme.

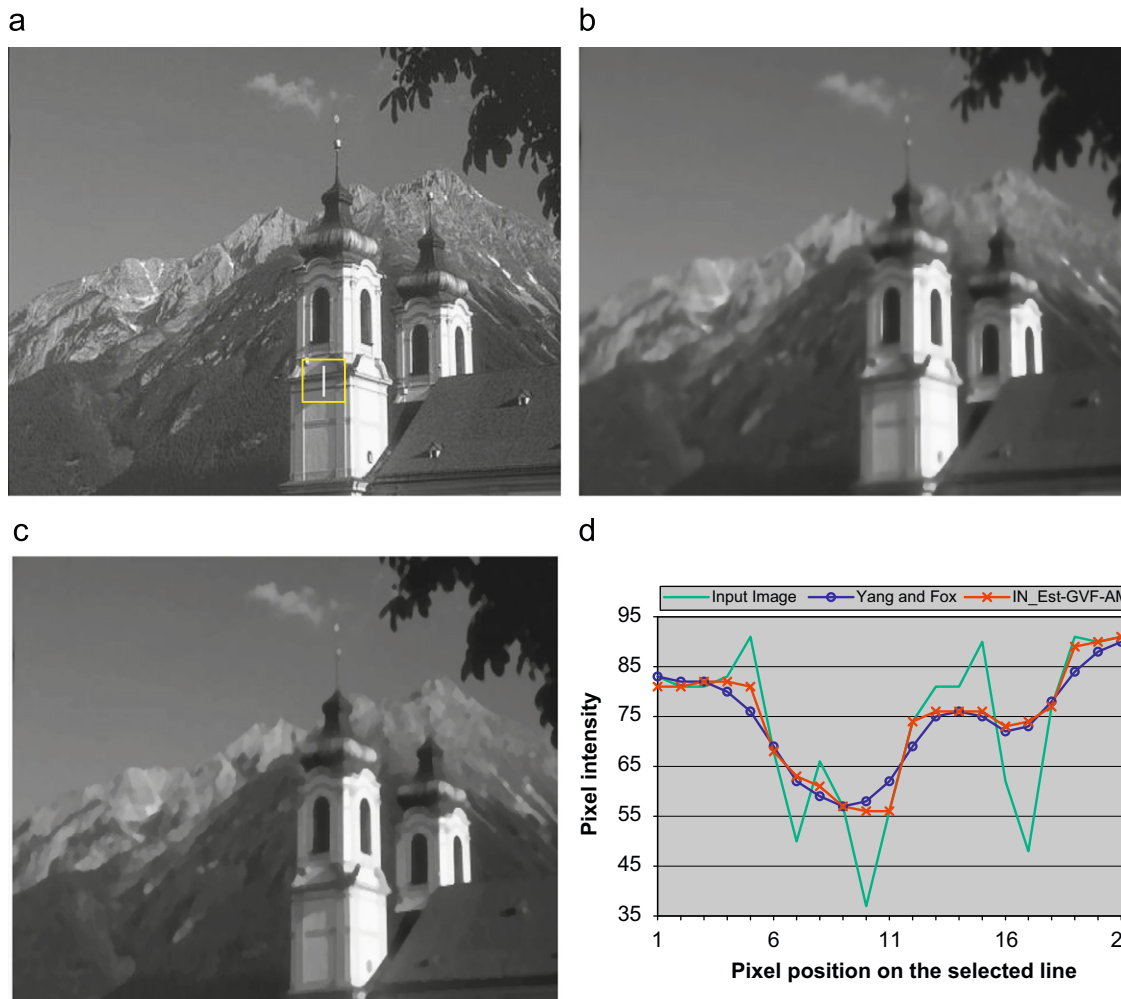


Fig. 11. (a) Original image [27]; (b) filtered image—Yang and Fox [22]; (c) filtered image— IN_{Est} -GVF-AM and (d) Pixel intensities plotted for the highlighted line depicted in image (a). Note the better edge preservation attained by the IN_{Est} -GVF-AM image restoration scheme.

they formulated the smoothing process in terms of the derivative of the flux function as follows:

$$I_t = \nabla(g(|\nabla I|)\nabla I), \quad I(t=0) = f, \quad \text{Newman conditions} \quad (13)$$

where $g(\cdot)$ is a monotonically decreasing function. The Perona–Malik (P–M) equation implements the diffusion process by performing aggressive smoothing in image areas defined by weak gradients and stopping the smoothing process at image regions defined by strong gradients. The P–M equation has received a significant amount of interest over the past two decades and numerous studies have been devoted to propose different mathematical models that either address the optimal implementation of the diffusion function $g(\cdot)$ [7,9,11] or improve its numerical stability around singular points [8,13,24]. While the anisotropic diffusion process is described in terms of PDE models, most of the efforts were concentrated on the development of mathematical schemes that are able to adjust the diffusion coefficients to the local image content. One such example is represented by the incorporation of the GVF field into the development of anisotropic diffusion models and this issue has been addressed in detail in the paper by Yu and Chua [23]. In this paper we will further analyse this approach and our study will be in particular concerned with the incorporation of the proposed IN_{Est} -GVF field in the development of an image restoration scheme with a view of

improving the performance of the filtering process in the presence of impulse noise.

3.1. Alvarez–Mazora formulation

The P–M anisotropic diffusion may be viewed as the solution of the heat conduction equation where the diffusion coefficient can be considered independent of space location. Building on this concept, Alvarez and Mazora (A–M) [1] reformulated the image restoration in terms of two coupled anisotropic diffusion models as follows:

$$I_t = -\text{sign}(G_\sigma * I_{\eta\eta})|\nabla f| + cI_{\varepsilon\varepsilon}, \quad I(t=0) = f \quad (14)$$

$$I_{\eta\eta} = \langle H^2 I \frac{\nabla I}{|\nabla I|}, \frac{\nabla I}{|\nabla I|} \rangle \quad \text{and} \quad I_{\varepsilon\varepsilon} = |\nabla I| \text{div} \left(\frac{\nabla I}{|\nabla I|} \right) \quad (15)$$

where $*$ is the convolution operator, η is the direction of the gradient, ε is the direction orthogonal to the gradient, c is a positive term, $\langle \rangle$ defines the dot product, H^2 is the Hessian matrix and div is the divergence operator. It can be observed that the first term in (14) defines a shock filter [17] that implements an inverse diffusive process. The aim of the shock filter is to perform a deblurring process between areas defined by zero-crossings of the smoothed second

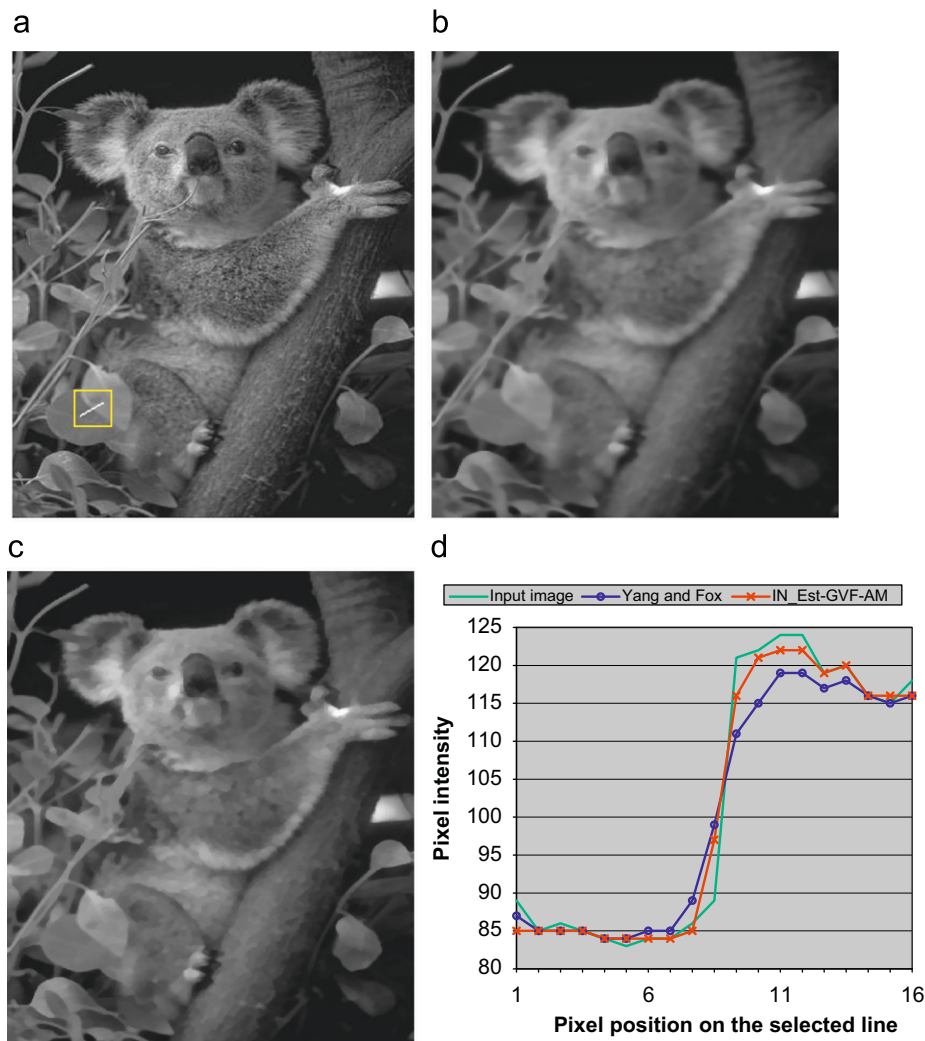


Fig. 12. (a) Original image [27]; (b) filtered image—Yang and Fox [22]; (c) filtered image— IN_{Est} -GVF-AM; (d) Pixel intensities plotted for the highlighted line depicted in image (a). Note the better edge preservation attained by the IN_{Est} -GVF-AM image restoration scheme.

derivative in the direction of the gradient. The second term implements a forward isotropic diffusion process along the isophotes and it has the role to smooth the noise in relatively flat image regions. This formulation produces superior results when compared to the standard P–M equation, but it is important to note that the A–M formulation is highly sensitive to noise as it is based on the calculation of the second order derivatives. This is the main motivation behind the introduction of the GVF field in the development of inverse and forward diffusion models, as the GVF field basically implements a weighted gradient diffusion process. Based on this observation, Yu and Chua [23] introduced the GVF field in equation (14) as follows:

$$I_t = -\text{sign}\left(\left\langle V, \frac{\nabla I}{|\nabla I|} \right\rangle\right) |\nabla f| + g(|\nabla I|) \Delta I, \quad I(t=0) = f \quad (16)$$

where V is the GVF field that is calculated using (1). In their paper, Yu and Chua [23] not only demonstrated that (16) leads to superior results when compared to (14), but also they have shown that (16) reaches the steady state solution more quickly than the original A–M equation. However, in their paper Yu and Chua did not analyse the stability of the image restoration scheme detailed in (16) when applied to data corrupted by impulse or mixed noise. Since the gradient information ∇I is used in the calculation of the inverse (shock) and forward diffusion components in (16), the GVF-based A–M anisotropic diffusion shows significant instability in the presence of impulse noise.

To compensate for this issue we propose a new formulation where the terms that implement the inverse and forward diffusion models are coupled with another term that implements

an adaptive median filter [14]. The combination between the median and anisotropic diffusion has been explored before by Yang and Fox [22] where the authors simply performed a weighted sum between the output of the median filter and the output of the A–M anisotropic diffusion term. Nonetheless, this approach is not appropriate since this noise removal scheme indeed attenuates the amplitude of the impulse noise in the filtered output, but this advantage is attained at the expense of weak feature preservation. Another disadvantage is related to the optimal selection of the parameter that weights the contribution of the median filter in the overall filtering process. In the implementation proposed by Yang and Fox [22] this weight is a user-defined parameter. To circumvent these undesirable effects, we propose the following coupled formulation:

$$I_t = (1 - IN_{Est}(f))(med(f) - I_t) + IN_{Est}(f) \left[-\text{sign}\left(\left\langle V_{IN_{Est}}, \frac{\nabla I}{|\nabla I|} \right\rangle\right) + g(|\nabla I|) \Delta I \right] \quad (17)$$

where IN_{Est} is the impulse estimator defined in (7), med is the adaptive median filter and $V_{IN_{Est}}$ is the IN_{Est} -GVF field defined in (4). In order to analyse in detail the formulation shown in (17) we recall that IN_{Est} takes values close to zero when the image is corrupted by impulse noise. In this way, we note that the first term performs impulse noise cancelling as it couples the original image with the output of the median filter.

Proposition. *If the pixel with coordinates (i,j) is corrupted by impulse noise, then the output of the image enhancement process shown in (17) approximates the output of the median filter.*

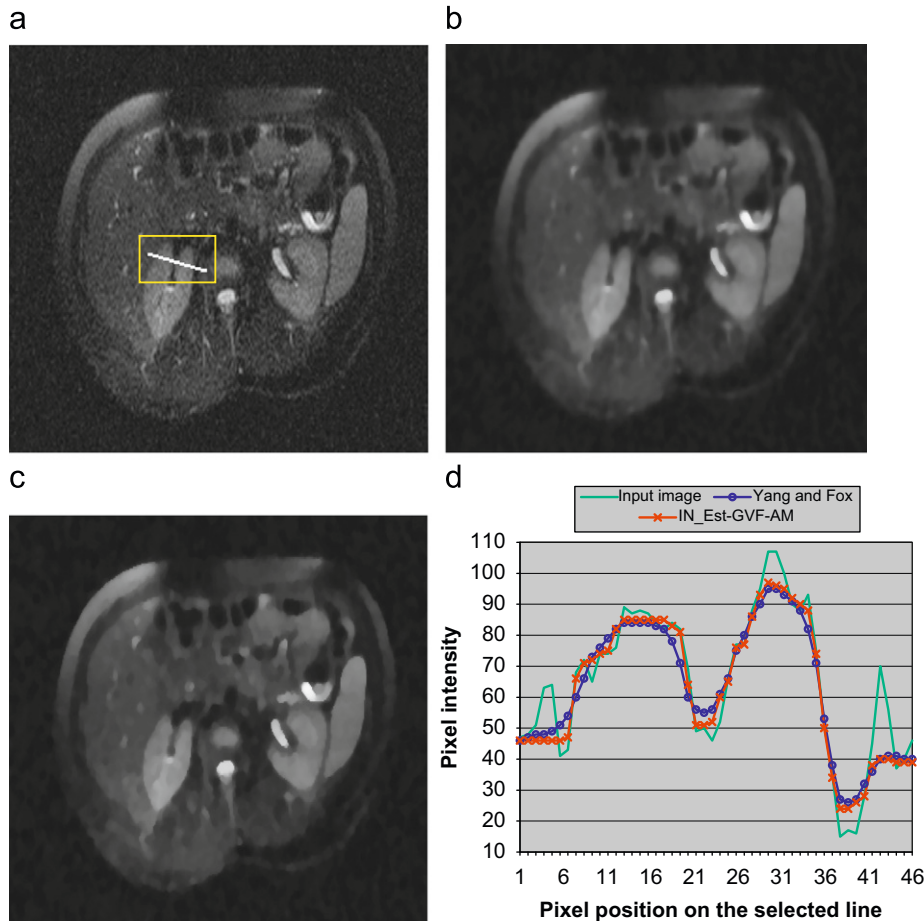


Fig. 13. (a) Original medical image [28]; (b) filtered image—Yang and Fox [22]; (c) filtered image— IN_{Est} -GVF-AM and (d) Pixel intensities plotted for the highlighted line depicted in image (a). Note the better edge preservation attained by the IN_{Est} -GVF-AM image restoration scheme.

Proof. If the pixel with coordinates (i,j) is corrupted by impulse noise ($IN_{Est}(f(i,j)) \approx 0$) and the time step $\Delta t = 1$, then the discrete implementation of (17) becomes,

$$I^{n+1}(i,j) = I^n(i,j) + med(f(i,j),\delta) - I^n(i,j) \Rightarrow I^{n+1}(i,j) = med(f(i,j),\delta) \quad (18)$$

where n is the iteration index and δ is the local neighbourhood where the median filtering is applied.

The second term of (17) implements the modified A–M equation depicted in (16) where the original GVF field has been replaced with the IN_{Est} -GVF field and for simplicity the diffusion function $g(\cdot)$ has been implemented using an exponential form $g(|\nabla I|) = \exp(-(|\nabla I|/k)^2)$, k being a diffusion parameter. As it can be observed in (17), the forward diffusion term dominates in the proposed IN_{Est} -GVF image restoration scheme in image areas defined by relative homogenous intensity distributions that are corrupted by Gaussian noise ($IN_{Est} \approx 1$) whereas the first term dominates in image areas corrupted by impulse noise ($IN_{Est} \approx 0$). □

4. Experimental results

The first set of experimental results aims to demonstrate the improved performance of the proposed image restoration formulation detailed in (17) when compared to the original GVF-based anisotropic diffusion proposed by Yu and Chua [23] when

applied to image data corrupted by Gaussian noise, impulse noise and mixed noise. To evaluate numerically the performance of the proposed formulation, the experimental results are quantified using the peak-signal-to-noise-ratio (PSNR).

$$PSNR = 10 \log_{10} \frac{\max(I(x))_{x \in \Omega}^2}{\frac{1}{size(\Omega)} \int \int_{(i,j) \in \Omega} (I(i,j) - O(i,j))^2 didj} \quad (19)$$

where Ω is the \mathbf{R}^2 image domain, $O(i,j)$ defines the pixel intensities of the original (noiseless) image and $I(i,j)$ are the pixel intensities resulting after the image restoration algorithms are applied to the image that is corrupted with noise. In all experiments conducted in this section the GVF field parameters have been set to the following values: $\mu=0.2$ (all GVF forms), $K=0.05$ (G-GVF) and $\Gamma=3 \times 3$ (IN_{Est} -GVF). The diffusion parameter k is set to 0.1 (function $g(\cdot)$ in Eqs. (16) and (17)).

As mentioned earlier the initial tests are conducted on data that is corrupted with Gaussian noise, visual and numerical results are depicted in Figs. 5–7.

The experimental results depicted in Figs. 5–7 indicate that all GVF-based A–M image restoration schemes analysed in this paper produce similar results when applied to data corrupted by low levels of noise. When the level of the Gaussian noise is increased, the proposed scheme (IN_{Est} -GVF-AM) produces more consistent results than the standard and the generalized GVF-AM

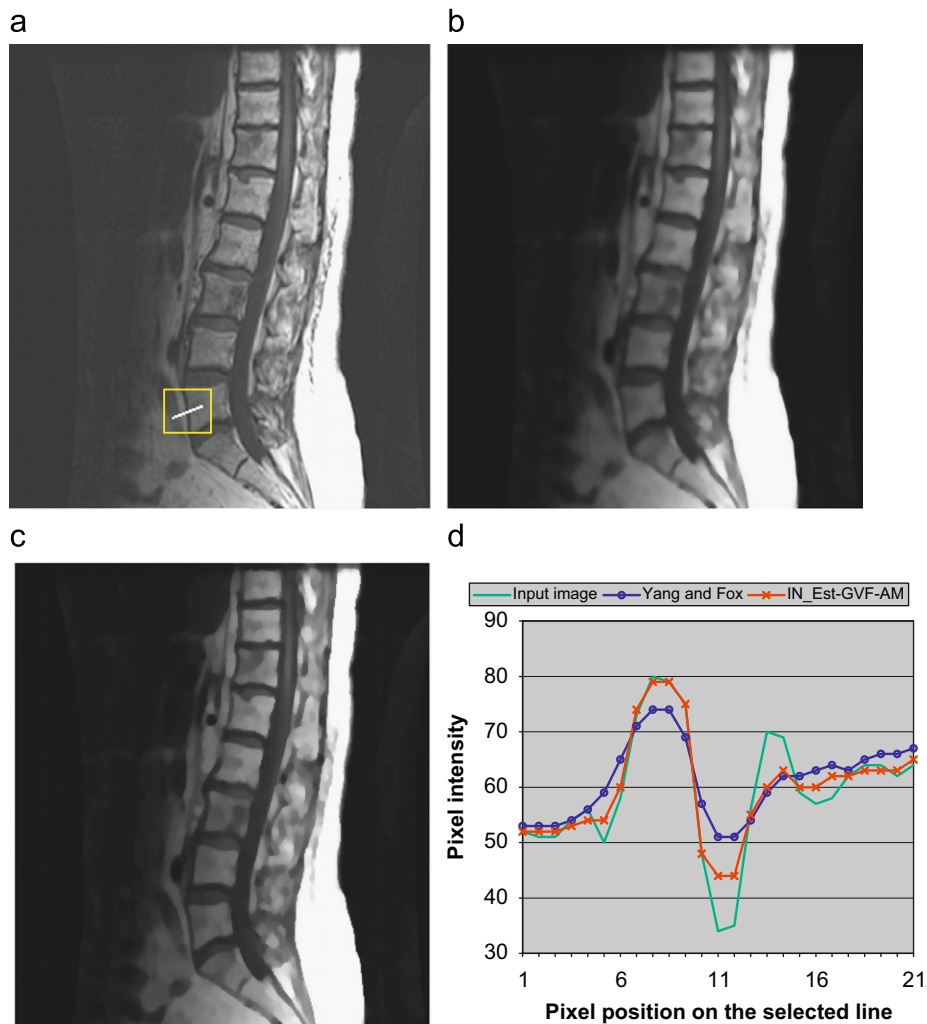


Fig. 14. (a) Original medical image [29]; (b) filtered image—Yang and Fox [22]; (c) filtered image— IN_{Est} -GVF-AM and (d) Pixel intensities plotted for the highlighted line depicted in image (a). Note the better edge preservation attained by the IN_{Est} -GVF-AM image restoration scheme.

approaches. These results were motivated by the vulnerability of the shock filter to high levels of image noise. The improved performance of the proposed scheme was expected since the regularized IN_{Est} -GVF leads to more stable fields in the presence of strong noise.

The second set of experiments has been conducted to evaluate the performance of the analysed image enhancement scheme when applied to data corrupted by impulse noise. A number of experimental results are shown in Fig. 8.

As Fig. 8 illustrates, the image restoration schemes implemented using (16) are extremely vulnerable in the presence of impulse noise, while the proposed (IN_{Est} -GVF) strategy implemented using (17) is well able to accommodate the impulse noise. The third set of experiments was conducted on images corrupted by mixed noise [21] and results are shown in Fig. 9 (in this experiment only the image restoration scheme detailed in (17) is evaluated as the previous experiments demonstrated that the GVF-based schemes constructed using (16) are vulnerable in the presence of impulse noise). For comparative purposes, the results and the PSNR values obtained when the Yang and Fox [22]

method is applied to data corrupted by mixed noise are also included in Fig. 9. For visualisation purposes close-up details are shown in Fig. 10. The results depicted in Figs. 9 and 10 indicate that the Yang and Fox method [22] is also able to reject the mixed noise, but this advantage is obtained at the expense of increasing the level of image blur. On the other hand, the proposed technique (IN_{Est} -GVF-AM) generates crisper results where the contextual image features such as edges are better preserved. This observation is further enforced by the higher PSNR values obtained by the IN_{Est} -GVF-AM image restoration scheme. Additional results are shown in Figs. 11–14 where the performance of the Yang and Fox [22] and IN_{Est} -GVF-AM is analysed with respect to edge preservation. The experimental results illustrated in Figs. 11–14 demonstrate that the IN_{Est} -GVF-AM outperforms the Yang and Fox [22] image restoration technique with respect to intra-region smoothing and contextual feature preservation.

The last experiments were conducted to evaluate the contribution of the proposed IN_{Est} -GVF field when included in the development of texture enhancement algorithms [25,26]. In the



Fig. 15. Coherence-enhancing anisotropic diffusion (CEAD): (a) Weickert implementation [26] and IN_{Est} -GVF-based CEAD—iterations=1; (b) IN_{Est} -GVF-based CEAD—iterations=5; (c) IN_{Est} -GVF-based CEAD—iterations=10 and (d) IN_{Est} -GVF-based CEAD—iterations=15.

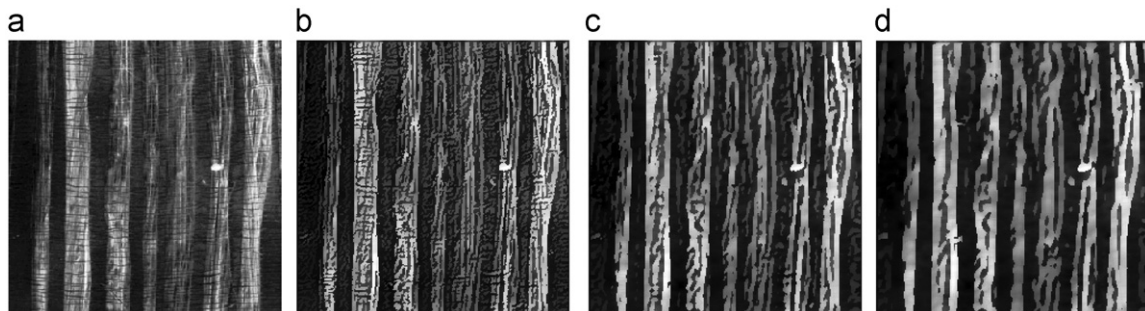


Fig. 16. Coherence-enhancing anisotropic diffusion (CEAD) when applied to a Brodatz [3] texture: (a) Original image; (b) Weickert implementation [26] and IN_{Est} -GVF-based CEAD—iterations=1; (c) IN_{Est} -GVF-based CEAD—iterations=5. (d) IN_{Est} -GVF-based CEAD—iterations=10.

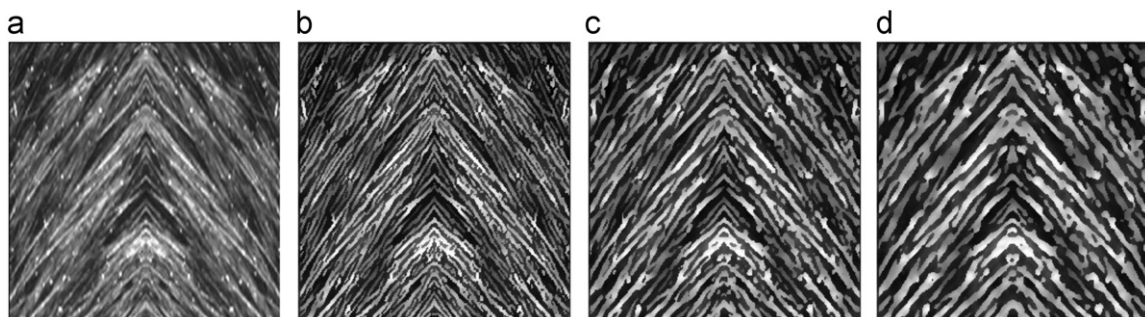


Fig. 17. Coherence-enhancing anisotropic diffusion (CEAD) when applied to a texture image characterised by strong orientation: (a) original image; (b) Weickert implementation [26] and IN_{Est} -GVF-based CEAD—iterations=1; (c) IN_{Est} -GVF-based CEAD—iterations=5 and (d) IN_{Est} -GVF-based CEAD—iterations=10.

remainder of this section we investigate the algorithm proposed by Weickert [26] where the structure tensor is included in the development of an anisotropic diffusion scheme that is able to enhance the coherent structures in the image. In this paper we have constructed the diffusion tensor using the IN_{Est} -GVF field and a number of experimental results are depicted in Figs. 15–17. The experimental results indicate that the application of the IN_{Est} -GVF field for texture enhancement is justified, as the edge diffusive process in the IN_{Est} -GVF field is applied in an iterative manner and the number of iterations controls the size of the neighbourhood where the coherent structures in the image are enhanced, as opposed to the original implementation [26]. It is useful to note that the proposed IN_{Est} -GVF-based algorithm generate the same results as those returned by Weickert's technique [26] when the GVF field is calculated using one iteration (i.e. $u(t=0)=f_x$, $v(t=0)=f_y$).

5. Conclusions

Due to its intrinsic properties, the GVF field is an attractive approach that can be applied in the development of image enhancement schemes. The standard GVF scheme proposed by Xu and Prince [19] is based on the evaluation of the second order derivatives and as a result this formulation shows severe instability in the presence of impulse noise. Thus, one of the aims of this work was focused on the development of a new GVF formulation where the gradient preservation term is regularized by the response of an impulse noise estimator. The new GVF-based formulation has been included in the development of a new image enhancement strategy that performs an adaptive coupling between the responses provided by the median and A–M anisotropic diffusion filtering schemes. The proposed scheme has been tested on image data corrupted by different types of noise and the experimental results indicate that the proposed image enhancement technique is able to better adapt to the characteristics of the image noise than the GVF-based A–M image filtering formulation proposed in [23]. Additional experiments have been conducted to illustrate the advantages associated with the proposed IN_{Est} -GVF field when incorporated in the development of texture enhancement algorithms. Our future studies will be focused on the evaluation of the proposed strategy when applied to practical cases such as the robust segmentation of multi-dimensional medical data.

Acknowledgements

This research was supported by NBIP Ireland funded under the HEA-PRTL Cycle 4, co-funded by the Irish Government and the European Union—Investing in your future. We would also like to thank the anonymous reviewers for their constructive comments.

Appendix A

As indicated in Section 2, the GVF is defined as the vector field that minimises the following functional:

$$\xi(V) = \int_{\Omega} \mu |\nabla V|^2 + |\nabla f|^2 (V - \nabla f)^2 d\Omega = \int \int_{(x,y) \in \Omega} F(x,y,V,V_x,V_y) dx dy \quad (A1)$$

where f is the input image, ∇ is the gradient operator, V_x , V_y are the partial derivatives of the GVF field V with respect to x and y axes and Ω is the two dimensional image domain. The minimisation of the functional $\xi(V)$ shown in (A1) can be performed using

the calculus of variations by applying the Euler–Lagrange equation as follows:

$$\frac{\partial F}{\partial V} - \frac{\partial}{\partial x} \frac{\partial F}{\partial V_x} - \frac{\partial}{\partial y} \frac{\partial F}{\partial V_y} = 0 \quad (A2)$$

If we calculate the partial derivatives of the function $F(\cdot)$ in equation (A2) (i.e.)

$$\frac{\partial F}{\partial V} = 2|\nabla f|^2 (V - \nabla f), \quad -\frac{\partial}{\partial x} \frac{\partial F}{\partial V_x} - \frac{\partial}{\partial y} \frac{\partial F}{\partial V_y} = -2\mu \Delta V$$

we obtain the following expression:

$$\mu \Delta V - |\nabla f|^2 (V - \nabla f) = 0 \quad (A3)$$

where Δ is the Laplacian operator. If we consider that the GVF field V is a function of the time variable t , then the functional depicted in (A1) takes the form of a first-order Hamilton–Jacobi and the solution of the equation shown in (A3) can be solved as follows:

$$\frac{\partial V(x,y,t)}{\partial t} + \min(\xi(V(x,y,t))) = 0 \quad (A4)$$

If we use the notation

$$V_t(x,y,t) = \frac{\partial V(x,y,t)}{\partial t}$$

then (A4) becomes,

$$V_t(x,y,t) = \mu \Delta V(x,y,t) - |\nabla f(x,y)|^2 (V(x,y,t) - \nabla f(x,y)) \quad (A5)$$

where the stationary values for $V(x,y,t) = [u(x,y,t), v(x,y,t)]$, $t \rightarrow \infty$ are the solutions of the Euler–Lagrange equation shown in (A3).

References

- [1] L. Alvarez, L. Mazora, Signal and image restoration using shock filters and anisotropic diffusion, *SIAM Journal of Numerical Analysis* 31 (2) (1994) 590–605.
- [2] M.J. Black, G. Sapiro, D.H. Marimont, D. Heeger, Robust anisotropic diffusion, *IEEE Transactions on Image Processing* 7 (3) (1998) 421–432.
- [3] P. Brodatz, *A Photographic Album for Artists and Designers*, Dover Publications, New York, 1966.
- [4] R.A. Carmona, S. Zhong, Adaptive smoothing respecting feature directions, *IEEE Transactions on Image Processing* 7 (3) (1998) 353–358.
- [5] F. Catte, P.L. Lions, J.M. Morel, T. Coll, Image selective smoothing and edge detection by non-linear diffusion, *SIAM Journal of Numerical Analysis* 29 (1) (1992) 182–193.
- [6] G.H. Cottet, L. Germain, Image processing through reaction combined with nonlinear diffusion, *Mathematics of Computation* 61 (1993) 659–673.
- [7] G. Gao, L. Zhao, J. Zhang, D. Zhou, J. Huang, A segmentation algorithm for SAR images based on the anisotropic heat diffusion equation, *Pattern Recognition* 41 (10) (2008) 3035–3043.
- [8] G. Gilboa, N. Sochen, Y. Zeevi, Forward-and-backward diffusion processes for adaptive image enhancement and denoising, *IEEE Transactions on Image Processing* 11 (7) (2002) 689–703.
- [9] G. Gilboa, N. Sochen, Y. Zeevi, Image enhancement and denoising by complex diffusion processes, *IEEE Transactions on Pattern Analysis and Machine Intelligence* 26 (8) (2004) 1020–1036.
- [10] O. Ghita, D.E. Ilea, P.F. Whelan, Image feature enhancement based on the time-controlled total variation flow formulation, *Pattern Recognition Letters* 30 (3) (2009) 314–320.
- [11] D.E. Ilea, P.F. Whelan, CTex – An adaptive unsupervised segmentation algorithm based on colour-texture coherence, *IEEE Transactions on Image Processing* 17(10) (2008) 1926–1939.
- [12] N. Jifeng, W. Chengke, L. Shigang, Y. Shuqin, NGVF: an improved external force field for active contour model, *Pattern Recognition Letters* 28 (1) (2007) 58–63.
- [13] H. Ling, A.C. Bovik, Smoothing low-SNR molecular images via anisotropic median-diffusion, *IEEE Transactions on Medical Imaging* 21 (4) (2002) 377–384.

- [14] R. Lukac, Adaptive vector median filtering, *Pattern Recognition Letters* 24 (2003) 1889–1899.
- [15] R. Malladi, J. Sethian, A unified approach to noise removal, image enhancement and shape recovery, *IEEE Transactions on Image Processing* 5 (11) (1996) 1554–1568.
- [16] A. Maalouf, P. Carre, B. Augereau, C.F. Fernandez-Maloigne, Cooperation of the partial differential equation methods and the wavelet transform for the segmentation of multivalued images, *Signal Processing: Image Communication* 23 (2008) 14–30.
- [17] S.J. Osher, L.I. Rudin, Feature-oriented image enhancement using shock filters, *SIAM Journal of Numerical Analysis* 27 (1990) 919–940.
- [18] P. Perona, J. Malik, Scale-space and edge detection using anisotropic diffusion, *IEEE Transactions on Pattern Analysis and Machine Intelligence* 12 (7) (1990) 629–639.
- [19] C. Xu, J.L. Prince, Snakes, shapes, and gradient vector flow, *IEEE Transactions on Image Processing* 7 (3) (1998) 359–369.
- [20] C. Xu, J.L. Prince, Generalized gradient vector flow external forces for active contours, *Signal Processing—An International Journal* 71 (2) (1998) 131–139.
- [21] Y. Xu, E.M. Lai, Restoration of images contaminated by mixed Gaussian and impulse noise using a recursive minimum–maximum method, *IEE Proceedings—Vision, Image and Signal Processing* 145 (4) (1998) 264–270.
- [22] Z. Yang, M.D. Fox, Speckle reduction and structure enhancement by multichannel median boosted anisotropic diffusion, *EURASIP Journal on Signal Processing* 16 (2004) 2492–2502.
- [23] H. Yu, C.S. Chua, GVF-based anisotropic diffusion models, *IEEE Transactions on Image Processing* 15 (6) (2006) 1517–1524.
- [24] G.Z. Yang, P. Burger, D.N. Firmin, S.R. Underwood, Structure adaptive anisotropic filtering, *Image and Vision Computing* 14 (1996) 135–145.
- [25] J. Weickert, Coherence-enhancing diffusion filtering, *International Journal of Computer Vision* 31 (2–3) (1999) 111–127.
- [26] J. Weickert, Multiscale texture enhancement, *Computer Analysis of Images and Patterns, LCNS*, vol. 970, Springer, Berlin, 1995, pp. 230–237.
- [27] The Berkeley Segmentation Dataset and Benchmark (BSD3), 2001. <<http://www.eecs.berkeley.edu/Research/Projects/CS/vision/grouping/segbench/>>.
- [28] Radiology Department, Mater Misericordiae Hospital, Dublin 7, Ireland.
- [29] Department of Radiology, University of Washington, Seattle, WA, USA.

About the Author—OVIDIU GHITA received the B.E. and M.E. degrees in Electrical Engineering from Transilvania University Brasov, Romania and the Ph.D. degree from Dublin City University, Ireland. From 1994 to 1996 he was an Assistant Lecturer in the Department of Electrical Engineering at Transilvania University. Since then he has been a member of the Vision Systems Group at Dublin City University (DCU) and currently he holds a position of DCU-Research Fellow. Dr. Ghita has authored and co-authored over 80 peer-reviewed research papers in areas of instrumentation, range acquisition, machine vision, texture analysis and medical imaging.

About the Author—PAUL F. WHELAN received his B.Eng. (Hons) degree from NIHED, M.Eng. from the University of Limerick, and his Ph.D. (Computer Vision) from the University of Wales, Cardiff, UK (Cardiff University). During the period 1985–1990 he was employed by Industrial and Scientific Imaging Ltd and later Westinghouse (WESL), where he was involved in the research and development of high-speed computer vision systems. He was appointed to the School of Electronic Engineering, Dublin City University (DCU) in 1990 and is currently Professor of Computer Vision (Personal Chair). Prof. Whelan founded the Vision Systems Group in 1990 and the Centre for Image Processing & Analysis in 2006 and currently serves as its director.

As well as publishing over 150 peer reviewed papers, Prof. Whelan has co-authored 2 monographs and co-edited 3 books. His research interests include image segmentation, and its associated quantitative analysis with applications in computer/machine vision and medical imaging. He is a Senior Member of the IEEE, a Chartered Engineer and a member of the IET and IAPR. He served as a member of the governing board (1998–2007) of the *International Association for Pattern Recognition* (IAPR), a member of the *International Federation of Classification Societies* (IFCS) council and President (1998–2007) of the *Irish Pattern Recognition and Classification Society* (IPRCS). Prof. Whelan is an HEA-PRTL (RINCE, NBIP) and SFI funded principal investigator.